J Mater Sci (2007) 42:7478–7487
DOI 10.1007/s10853-006-1462-0

Material properties of portland cement paste with nano-montmorillonite

Ta-Peng Chang · Jeng-Ywan Shih · Kuo-Ming Yang · Tien-Chin Hsiao

Received: 18 April 2006 / Accepted: 15 December 2006 / Published online: 18 May 2007

Abstract The nano-montmorillonite, which has characteristics of high aspect ratio and interaction between polymer chains and dispersed nanolayers, has been widely used in the development of new reinforced nanocomposite polymers to improve their mechanical properties. Since a potential pozzolanic reaction may occur between Portland cement paste and high amount of silicon dioxide (SiO_2) in nano-montmorillonite, the effects of introduction of montmorillonite to Portland cement-based material on the improvement of matrix properties of cement paste is of great interest in the construction industry. In this study, a liquid-form of nano-montmorillonite particle with a planar diameter of about 100 nm were incorporated into the Portland cement paste at five different dosages and analyzed at four different ages to identify the nanosizing effects on material properties of such cement-based composite. Experimental results show that the composite with 0.60% and 0.40% of added nano-montmorillonite by weight of cement have the optimum compressive strength and permeability coefficient, respectively, in which the increase of compressive strength is about 13.24%, and the decrease of permeability coefficient about 49.95%. Microstructural properties through the analyses of XRD, DSC, NMR, and MIP also indicate that the microstructures of cement paste with nano-montmorillonite contain more dense solid material and more stable bonding framework.

T.-P. Chang (✉) · J.-Y. Shih · K.-M. Yang · T.-C. Hsiao
Department of Construction Engineering, National Taiwan University of Science and Technology, 106, Taipei, Taiwan, R.O.C.
e-mail: tpchang@mail.ntust.edu.tw

T.-C. Hsiao
Department of Interior Design, China University of Technology, 106, Taipei, Taiwan, R.O.C.

Introduction

Nanoscience and nanotechnology refer to the exploration, innovation, and application of nanomaterials, which are characterized by at least one dimension in the nanometer (nm) range. The size range that evokes greatly attention is below 100 nm, and properties of materials in such nanoscale differ from those of the atomic or the bulk materials of same composition [1, 2]. Natural nanomaterials mostly appear as fine particulate minerals near Earth surface, for example. clay minerals perform size-dependent properties that make them roles for lots of utilizations [3].

Nano-montmorillonite (NM) is the most common member of smectite clay family, which is sometimes referred to as ''nanoclay'', and belongs to general mineral group of clays, whose particle's shape consisting of a sheet-like structure where the dimensions in two directions far exceed its thickness. Basically, it consists of a three-layered structure of aluminum sandwiched between two layers of silicon, similar to the mica-type layered silicates. Montmorillonite is an active and major ingredient in a volcanic ash called bentonite which has an ability to swell to many times its original weight and volume when it absorbs water. Thus, in engineering application, it is often mixed with water to give water higher viscosity and used as the drilling muds in removing drill debris of foundation excavation of civil constructions such as slurry wall, earth dam, etc. [4, 5]. In 1987, the techniques of cation exchange and intercalated polymerization were utilized for the first

time to make a sheet-like nano-montmorillonite with 1-nm thick individual layers and 100–1000 nm wide in platey dimensions and dispersed in nylon 6 matrix [6]. Since then, the engineering application of nano-montmorillonite has been enhanced from the traditional stabilizing drilling mud to some advanced utilizations like nanocomposites commonly used in the industry fields. Furthermore, the nano-sized particles of nano-montmorillonite minerals are dispersed in polymers to create new class of reinforced nanocomposite materials that offer improved performance and mechanical properties such as strength, modulus of elasticity and thermal stability, but other properties such as toughness and impact resistance may be reduced [7, 8]. Such nanocomposite is a typical hybrid material combined with both organic and inorganic compounds. In general, three main types of such composites can be obtained when a layered nanomaterial is incorporated into polymers:(1) phase separated microcomposite; (2) intercalated nanocomposite and (3) exfoliated nanocomposite [9]. For the phase-separated microcomposite, the included nanomaterial maintains its original multilayered structure and is distributed uniformly in the polymers as the conventional composites. When the well ordered multilayered nanomaterial in polymers is intercalated with the polymer chain to form alternating polymeric and inorganic layers, an intercalated nanocomposite is obtained. An exfoliated nanocomposite means that the multilayered nanomaterial in polymers is completely separated into layers and uniformly dispersed in continuous polymer matrix. Both techniques of transmission electronic spectroscopy (TEM) and X-ray diffraction analysis (XRD) can be used to identify these three nanocomposite structures [10].

On the other hand, the microstructure of hydrated Portland cement paste is mainly composed of calcium silicate hydrate gel (xCaO· ySiO$_2$· mH$_2$O, which is usually abbreviated as C–S–H), calcium hydroxide (Ca(OH)$_2$), ettringite ($C_6A\bar{S}_3H_{32}$) and calcium aluminate monosulfate hydrate ($C_4A\bar{S}H_{18}$) [11]. Among these four chemical compounds, the C–S–H, which is the hydration product formed from the reaction of calcium silicates in cement and water, provides major strength of the hydrated cement paste. The microstructures of C–S–H gels in an ordinary Portland cement (OPC) paste and a slag/OPC blend paste examined by high-resolution electron microscopy have shown that some nanocrystalline regions on the scale of 5 nm or less in C–S–H do exist in both cement paste composites [12]. Apparently, the nano-montmorillonite has a dimension of about 1 nm being in same order of the nanocrystalline microstructure of C–S–H. Meanwhile, nano-montmorillonite had been reported as a fairly good pozzolanic material [13]. It is of practical importance to characterize the role of nano-montmorillonite in the matrix of cement paste composite resulting from effects of its dispersion and pozzolanic reaction. Literature review has indicated that studies on this subject are very limited. The present investigation is aimed at studying the material properties and microstructures of the nanocomposite consisting of these two inorganic materials, Portland cement paste and nano-montmorillonite. In addition to using the compressive strength and permeability as two major indices to explore the material properties, other physical properties such as the thermal behavior, degree of hydration and fractal dimension are also addressed in this study.

Experimental program

Material, experimental variable and specimen

Portland cement complying with ASTM C150 standard and ordinary tap water were used as mixing materials for the cement paste. Chemical compositions and physical properties of ASTM Type I Portland cement are given in Table 1. Nano-montmorillonite (NM) in liquid form purchased from J Nano Technology Co., Ltd. was used as the admixture, whose physical properties are given in Table 2. After some preliminary trial tests, the water/cement (W/C) ratio was fixed at 0.55, from which five different dosages of nano-montmorillonite, 0.0, 0.2, 0.4, 0.6 and 0.8% of cement weight were added to the mix to make the specimens of cement paste nanocomposite. The mix proportions of these nanocomposites are given in Table 3. Two kinds of cylindrical nanocomposite specimens were used in the study: φ 25 × 50 mm specimen for the compressive test

Table 1 Chemical and physical properties of ASTM Type I Portland cement used in this study

Chemical composition (mass %)							
SiO_2	Al_2O_3	Fe_2O_3	CaO	MgO	SO_3	Free CaO	LOI
20.31	5.05	3.16	62.43	3.81	2.48	0.78	1.49
Physical properties							
Fineness (m^2/kg)		Specific gravity		Initial setting (minutes)		Final setting (minutes)	
349.0		3.15		185.0		292.0	

Table 2 Basic material properties of nano-montmorillonite (NM) (in liquid form)

Composition (mass%)	SiO_2 (72.4%), Al_2O_3 (17.0%), Fe_2O_3 (3.6%), other (7.0%)
Dimension	100 × 100 × 0.1 nm (platey shape)
pH value	10.0

Table 3 Mix proportion of Portland cement composite

Designation	Cement :water : NM (by mass)
C-00	1 : 0.55 : 0.000
C-02	1 : 0.55 : 0.002
C-04	1 : 0.55 : 0.004
C-06	1 : 0.55 : 0.006
C-08	1 : 0.55 : 0.008

and φ 100 × 200 mm specimen for the permeability test in which the middle portion of φ 100 × 200 mm specimens were cut by diamond saw into several slices with thickness of 10 mm for the test. Each experiment was performed at four ages of 7, 14, 28 and 56 days using three specimens prepared from same batch of mixture. All the specimens of cement paste nanocomposite were demoulded 24 h after they were cast and then immersed in saturated limewater basin until one day before the test and cured in ambient temperature for 24 h.

Experimental methods and facilities

Two-stage experimental stages were performed in this study. In the first stage, the compressive strength tests and permeability tests of nanocomposite specimens at four ages with five different added dosages of nano-montmorillonite were conducted and assessed to obtain the optimal mix proportion. The test of compressive strength of cylindrical nanocomposite specimen was performed by a 10-ton material testing machine following the procedure of ASTM C39 standard. The permeability coefficient of nanocomposite was determined by a gas permeability test to be described in details shortly in the following section. These two performance indices will be used as the fundamental criterion to select the optimal nanocomposite for the experiment in the second stage, from which, the microstructural properties of the optimal nanocomposite were examined with the following four different facilities:

(1) Mineralogy profiles measured by X-ray Diffractometer (XRD) using a Mac MO3X-HF (40 kV at 30 mA, and CuK radiation, λ = 0.1541 nm).
(2) Heat effects associated with phase transitions and chemical reactions as a function of temperature monitored by Differential Scanning Calorimetry (DSC) using a Netzsch Instrument HT-DSC 404 (20 °C to 1400 °C at 10 °C/min increment).
(3) Degree of hydration assessed by Nuclear Magnetic Resonance (NMR) using a Varian 400 MHz.
(4) Porosity analyzed by Mercury Intrusion Porosimeter (MIP) using a Micromeritics AutoPore IV 9520 (from atmospheric pressure to 414 MPa).

Permeability test

The permeability of concrete is one of the most important microstructural properties that are directly related to its long-term durability. Although there are several different techniques that can be used for measuring the permeability of cement composite, using a gas is one of the easiest and fastest methods. Various gases had been used as the permeating fluids, for instance, oxygen [14], nitrogen [15], ethanol vapor [16], and methanol vapor [17]. In this study, the gas permeability test following the proposed apparatus and approach by Alshamsi and Imran [17] was used to determine the permeability coefficient of nanocomposite. Three pieces of cylindrical disk specimen of φ 100 × 10 mm for each of five mix proportions at each of four ages were prepared for the test. The disk specimens were dried in oven at 105 °C for 24 h to remove the moisture within specimens and then placed and sealed on the top of a cell with silicon sealer to avoid leakage of methanol vapor as shown schematically in Fig. 1. The initial weight of whole specimen setup including the cell, methanol, liquid, φ 100 × 10 mm disk specimen and silicon rubber was measured at the beginning of the test. The values of mass variation versus time due to the vaporization of methanol liquid during the test were continuously recorded at each

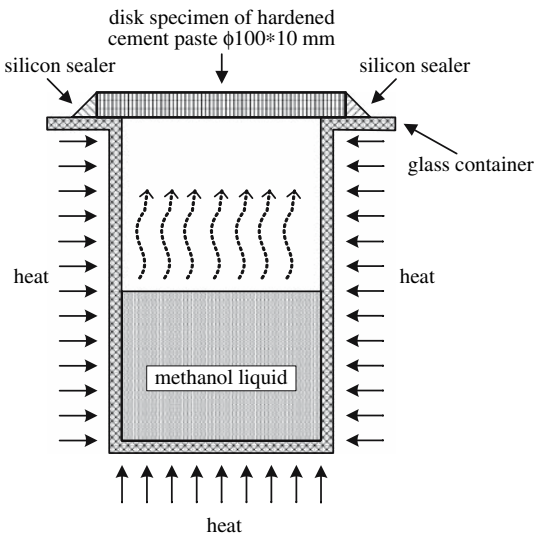

Fig. 1 Schematic diagram of sample preparation for gas permeability test

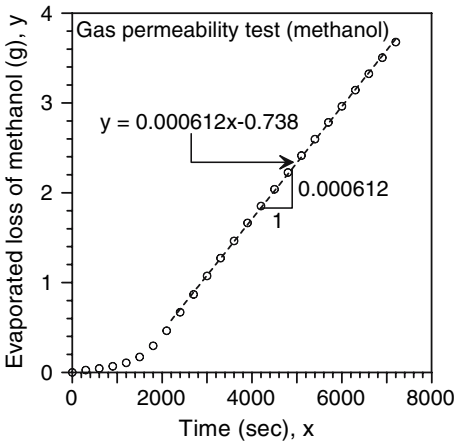

Fig. 2 Typical curve of time verse evaporated loss for gas permeability test

time interval until a steady-state mass loss was reached at about 2 h for each test in this study. A typical plot of gas permeability test is presented in Fig 2. The permeability coefficient of nanocomposite specimen was then calculated using the following equations [17, 18].

$$P_V = 10^{(8.0809-\frac{1582.2}{239.76+T})} \quad (1)$$

$$\eta = 10^{-7}\left(4.7169T^{0.618} - 99e^{-8.7593\times10^{-4}T} + 94e^{-7.916\times10^{-3}T} + 5\right) \quad (2)$$

$$Q = \frac{266\times10^{-3}\dot{m}T}{10^{(8.0809-\frac{1582.2}{239.76+T})}} \quad (3)$$

$$k = \frac{2L\eta P_2 Q}{A(P_1^2 - P_2^2)} \quad (4)$$

where P_V = the absolute pressure of vapor (N/m^2), T = the absolute temperature (°K), η = the dynamic viscosity (N s/m^2), Q = the volumetric flow rate (m^3/s), $\dot{m}$ = the rate of mass loss (g/s), k = the intrinsic permeability coefficient (m^2), P_1 = the inlet pressure (N/m^2), P_2 = the outlet pressure (N/m^2), L = the length of the sample (m) and A = the cross-sectional area perpendicular to the flow direction (m^2).

Results and discussion

Properties of nano-montmorillonite

The nano-montmorillonite was examined by both TEM and XRD as shown in Figs. 3 and 4. The TEM micrograph in Fig. 3 indicates that the dimension of platey microstructure of nano-montmorillonite of 100 × 100 × 1 nm belongs to the range of nanoscales. The XRD pattern in Fig. 4 shows a broader diffraction peak with the highest value occurred at

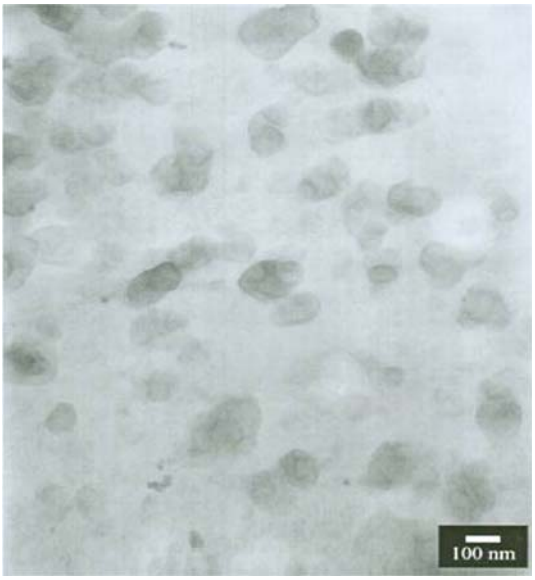

Fig. 3 TEM micrograph of nano-montmorillonite

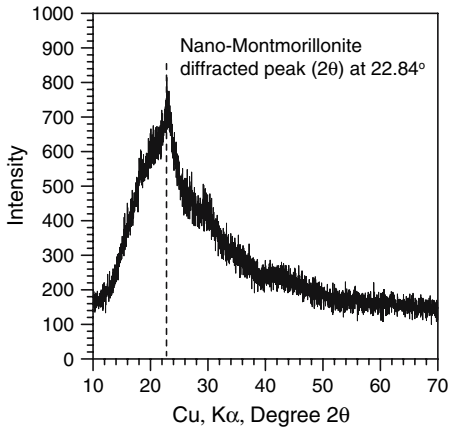

Fig. 4 X-ray diffraction (XRD) pattern of nano-montmorillonite

2θ = 22.84 ° which also implies that nano-montmorillonite belongs to an amorphous substance having a poor crystalline structure. From Brag law $2d\sin\theta = n\lambda$, it can be found that its lamellar repeat distance is about 0.389 nm.

Properties of harden cement paste

Compressive strengths

Test results of compressive strengths of the cement paste composite with four additions of NM at four ages are given in Fig. 5, in which an optimum value of about 0.6% is obtained. Among all the curves of strength development, the highest percentage of strength increase is only about 13.24% for C-06 curve occurring at age of 56 days. Basically, the effects of NM addition on mechanical properties

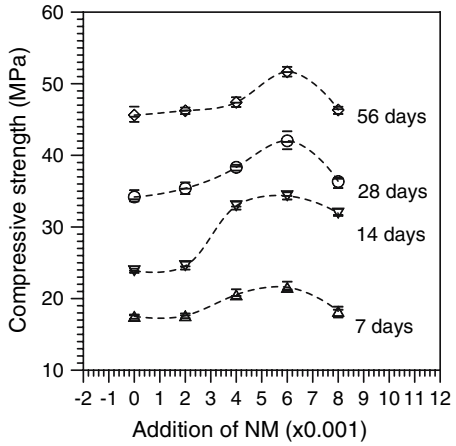

Fig. 5 Compressive strengths of cement paste at various additions of NM and ages

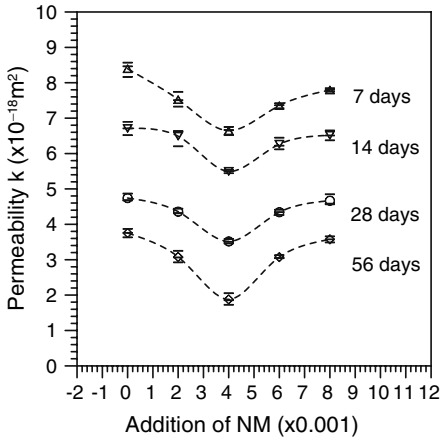

Fig. 6 Permeability coefficients of cement paste at various additions of NM and ages

of the cement paste composite can be roughly divided into two types, one is the filling effect into the porosity of the microstructure of hydrated cement paste composite and the other is the effect of supplementary chemical interaction such as pozzolanic reaction reacted with those major oxide compounds of Type I Portland cement, such as CaO, SiO_2, Al_2O_3 and Fe_2O_3. A small increase of compressive strength in this case indicates that although some additional chemical strong bonding due to the addition of NM resulting from the latter effect can be expected, the former filling effect seems to prevail. Microstructural examination on those hardened cement paste composite to be deliberated shortly in the next sections will be used to assess this macro-behavior.

Permeability coefficient

Test results of permeability coefficients of cement paste composite, k, with four additions of NM at four ages are given in Fig. 6, which shows an apparent optimum value of 0.4% for all ages. By comparing with the control set (C-00 curve), it can be found that the highest percentage of decrease of permeability coefficient is about 49.95% for C-04 curve occurring at age of 56 days. In contrast to a small percentage of 13.24% increase of compressive strength, apparently, the effects of NM on blocking the permeability paths of cement paste composite due to gas diffusion seem to be more significant.

Microstructural examination on performance of nano-montmorillonite in cement paste composite

Based on experimental results of compressive strength given in the previous sections, the hardened cement paste composite with an optimum addition of 0.6% of nano-montmorillonite at age of 56 days was selected for the performance analysis by the microstructural examination, which, in turn, can be served as a base to evaluate the controlling conditions on the effectiveness of addition of nano-montmorillonite. As a comparison, the microstructural examination on the hardened pure cement paste at age of 56 days was also conducted in this study.

XRD examination

The composition of CH has a well-defined crystallized structure. According to the data bank of JCPDS PDF 44–1481 [19], it has four major peaks in the XRD pattern that corresponds to 2θ of 18.00°, 34.10°, 47.12° and 50.81°, and crystal planes of Miller indices (hkl) of (001), (101), (102) and (110), respectively. Test results of XRD examination for CH are shown in Fig. 7a, b and Table 4, respectively. Comparison of 2θ of these two figures with that of PDF 44–1481 indicates that the four peaks in these two XRD patterns indeed represent the existence of CH. The diffracted intensity of 183.0 in the crystal plane of (001) in Fig. 7a reduces by 10.93% as compared with that of 163.0 in Fig. 7b. indicating an obvious consumption of CH mainly due to the effect of pozzolanic reaction in the presence of NM. Also, referred to both PDF 36–0642 and PDF 42–0551 [19], the microstructures of tricalcium silicate (C_3S) and dicalcium silicate (C_2S) exist at 2θ from 29° to 35° of XRD. These two figures confirm this result, although the peaks are not obviously perceivable. After the addition of NM, intensities of C_3S and C_2S of the hardened Portland cement paste also become smaller as a result of the production of C–S–H from the pozzolanic reaction.

DSC examination

Figure 8a and b show that four endothermal peaks appear around 100 °C, 470 °C, 720 °C and 1300 °C, corresponding to temperatures of the vaporization of capillary water,

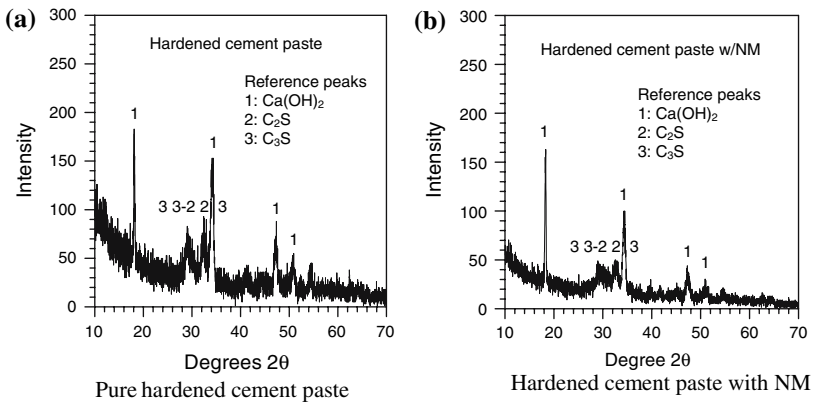

Fig. 7 Typical XRD patterns of hardened Portland cement paste (**a**) without NM (**b**) with 0.6% added NM

Table 4 Test results of XRD examination for calcium hydroxide (CH)

Item	Miller index							
	(001)		(101)		(102)		(110)	
	2θ	I^*	2θ	I^*	2θ	I^*	2θ	I^*
JCPDS data bank	18.00°	–	34.10°	–	47.12°	–	50.81°	–
Pure cement paste	18.10°	183.0	34.14°	153.0	47.36°	88.0	50.92°	55.0
Cement paste with NM	18.34°	163.0	34.34°	100.0	47.28°	44.0	50.92°	31.0

Note: I^* = intensity

dehydroxylation of CH and decarbonation of calcium carbonate, respectively [20, 21]. The last temperature corresponds to the glass-transition temperature (T_g) that transforms the phases of specimen from a powder into a melted substance after the experiment was done [22]. The peak of CH variation appears to be the sharpest. The difference between two temperatures of 469.63 °C and 470.62 °C on the dehydroxylation of CH for two types of hardened cement pastes is only about 1 °C, while the T_g temperature raises from 1296.62 °C to 1301.78 °C by an increase of about 5 °C, indicating that the cement-based composite with NM seems to have higher melting point.

NMR examination

Magic-angle spinning nuclear magnetic resonance (NMR) measurements have been performed on ^{29}Si nuclei for Portland cement powder, pure hardened Portland cement paste and hardened Portland cement composite with NM as shown in Figs. 9, 10a and b, respectively. In the NMR analysis, since the differences in resonance frequencies are very small, the difference is normally measured between the substance to be analyzed and a reference compound. The most common reference is tetramethylsilane $(CH_3)_4Si$, also called TMS. The chemical shift from TMS is in the

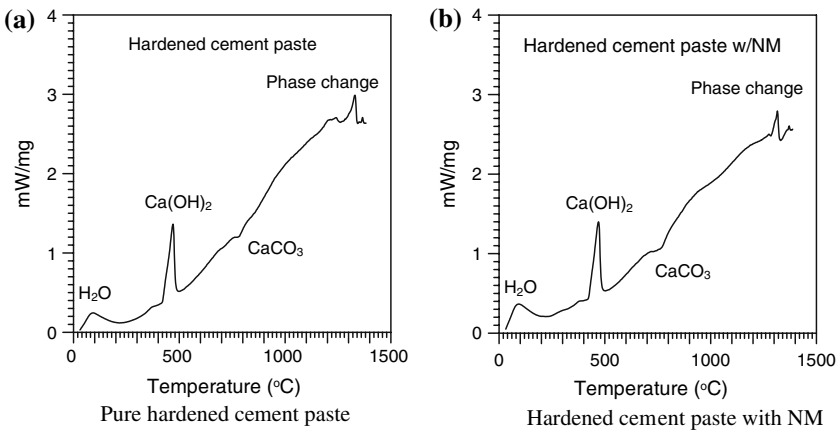

Fig. 8 Typical DSC curves of hardened Portland cement paste (**a**) without NM (**b**) with 0.6% added NM

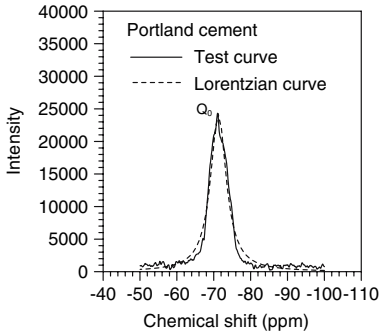

Fig. 9 Typical NMR curve of Portland cement

units of ppm. Let Q^n represent the different shift zones of ^{29}Si, where Q is the silicate tetrahedron and n refers to the number of bridging oxygens. The peaks appear around –70, –80, –88, –98 and –110 pm are then referred to as Q^0, Q^1, Q^2, Q^3 and Q^4 [23]. Fig. 12 has a single peak of Q^0, while Fig. 13a and b have two peaks of a narrow peak of Q^0 and a wider peak for both Q^1 and Q^2. Neither Q^3 nor Q^4 in these figures was observed.

Quantitative analysis of these peak values can be obtained through either Gaussian function or Lorentzian function [23]. The former has a symmetric curve with a rapid descending tail, while the latter has a relatively slow descending that seems to match the experimental data better and thus is adopted in this analysis. The Lorentzian function y can be expressed as follows [24].

$$y(x) = y_0 + \frac{2A}{\pi} \times \frac{W}{4(x - x_c)^2 + W^2} \tag{5}$$

where y_0 is the datum of the peak, A the area covered by the peak, x_c the location of peak and W the full-width-at-half-maximum (FWHM). Least-square fitting of Lorentzian function to obtain values of four parameters y_0, A, x_c and W of NMR curves was carried out. These four values are given in Table 5 with coefficients of determination of R^2 of 0.972, 0.989 and 0.986, respectively. Their corresponding curves are also plotted in Figs. 9, 10a and b, respectively.

The values of Q^0 for Portland cement powder, hardened Portland cement paste and hardened Portland cement composite are –71.26, –71.06 and –71.22 ppm, respectively, which are slightly lower than –70 ppm. The values of Q^1 and Q^2 for hardened Portland cement paste and hardened Portland cement composite are –79.48, and –79.85 ppm closed to –80 ppm, and –84.05 and –84.28 ppm higher than –88 ppm, respectively. The variation of Q^0 can be used to estimate the degree of hydration for the cement-based composite, α, through the following equation [25].

$$\alpha = \left[1 - \frac{I(Q^0)}{I^0(Q^0)}\right] \times 100\% \tag{6}$$

where $I(Q^0)$ is the value of Q^0 in the hydrated cement-based composite and $I^0(Q^0)$ the value of Q^0 in the Portland cement powder. Substituting values of Q^0 of cement past and cement composite with NM into Eq. (6) gives values of α of 70.38% and 72.34%, respectively. At age of 56 days, the degree of hydration of hardened cement composite with NM increases by about 2% by comparison with the hardened cement paste. The index of Q^2/Q^1also refers to the characteristics of cement composite in which a higher value indicates a better mechanical property [26]. The addition of NM into cement paste increases the value of Q^2/Q^1 from 0.0806 to 0.2227, which in turn increases the compressive strengths and reduces the permeability coefficient of cement composite as stated in the previous section. In addition, the variation of FWHM of Q^n peaks in NMR is also of interesting to observe the pattern of microstructure, in which a wider FWHM implies more irregular microstructure [27]. After hydration, the difference of FWHM of Q^0 peak as shown in Figs. 9, 10a and b is minor regardless of whether the NM is present or not. However, after addition of NM, FWHM value of Q^1 peak in the cement composite reduces substantially by about 22.13% while FWHM value of Q^2 peak increases slightly. As a result, the arrangement order of –O–Si–O net tends to become regular with a pattern of sharing a common oxygen atom. As a whole, both the increases of α and $Q^2/Q^1$and the decrease

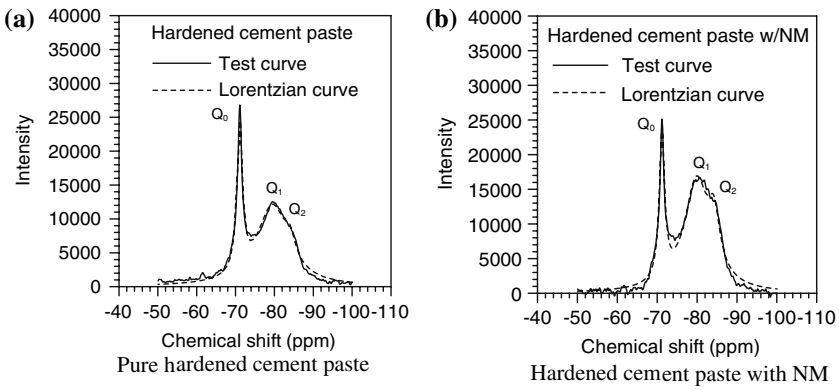

Fig. 10 Typical NMR curves of hardened Portland cement paste (**a**) without NM (**b**) with 0.6% added NM

Table 5 Values of constants of Lorentzian functions from NMR curve fitting

	Portland cement powder	Pure hardened Portland cement paste			Hardened Portland cement composite with NM		
Q^n	Q^0	Q^0	Q^1	Q^2	Q^0	Q^1	Q^2
y_0	0		0			0	
x_c	–71.26	–71.06	–79.48	–84.05	–71.22	–79.85	–84.28
A	195769.26	57996.43	175894.72	14170.37	54140.64	184080.08	40992.43
W	5.15	1.65	9.58	3.12	1.66	7.46	3.53
R^2	0.972		0.989			0.986	

of FWHM indeed confirm the improvement of microstructures of hydrated cement composite as a result of addition of NM.

MIP examination

Mercury intrusion porosimetry (MIP) is a widely used method for approximately measuring the pore-size distribution of porous materials, in particular, cement-based materials. In the MIP method, non-wetting fluid of mercury is forced to penetrate into porous samples by the gradually increasing controlled pressures. Incremental pressures and volume variations of the intruding mercury are then carefully measured during the test to provide data on the estimation of volume and size of pores of the samples. Assuming cylindrical pores, the relation between applied pressure and pore size is given by the Washburn equation [28, 29]:

$$P = -\frac{4\gamma\cos\theta}{d} \tag{7}$$

where P is the applied pressure, γ is the mercury's surface tension, and θ is the contact angle of the mercury, d is the diameter of the cylindrical pore. A surface tension of 0.484 N/m and a contact angle of 117° of mercury were used in the Washburn equation (7) for cement paste to convert applied pressure to pore diameter from the experimental MIP data via the following equation [28–31]

$$d = 878.93/P \tag{8}$$

where d is the pore entry diameter in nm, P is the applied pressure in MPa.

Typical experimental MIP plots of cumulative pore volume verse pore diameter are shown in Fig. 11a and b, which show that total pore volume decreases by 4.10% from 0.244 ml/g for the pure hardened cement paste to 0.234 ml/g for the cement composite with 0.6% added NM. Other MIP plots of distributive pore volume verse pore diameter are presented in Figs. 12a and b, respectively, in which the pore size distribution shifts to finer pore sizes for cement composite with 0.6% added NM. Therefore, both indices of decrease of pore volume and smaller pore size distribution demonstrate that the hardened Portland cement composite with NM has a more consolidated microstructure.

Figure 13a and b show typical experimental curves of accumulated pore volume verse pore size d in log-log scale for both the Portland cement pastes with and without NM. Their corresponding liner regression lines are fitted by the following equation.

$$\log V^* = C + k\log d \tag{9}$$

where V^* is the volume ratio in percentage assuming the value of maximum pore entry diameter to be 100, and C and k are constants to be found. Then the value of constant

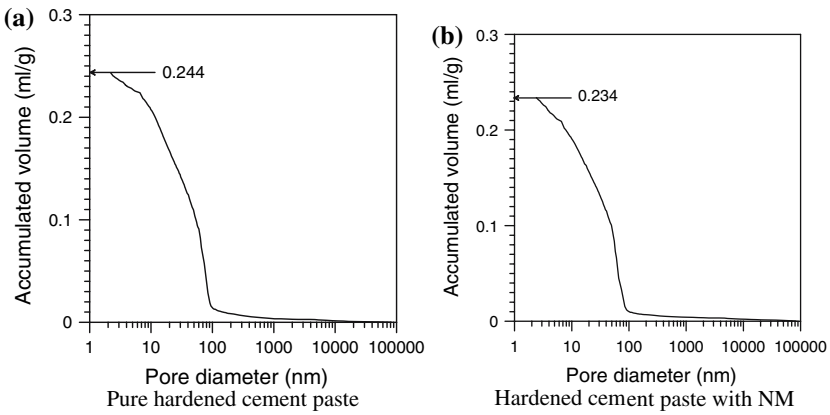

Fig. 11 Typical curves of accumulated MIP pore volume verse pore diameter for hardened Portland cement composite (**a**) without NM (**b**) with 0.6% added NM

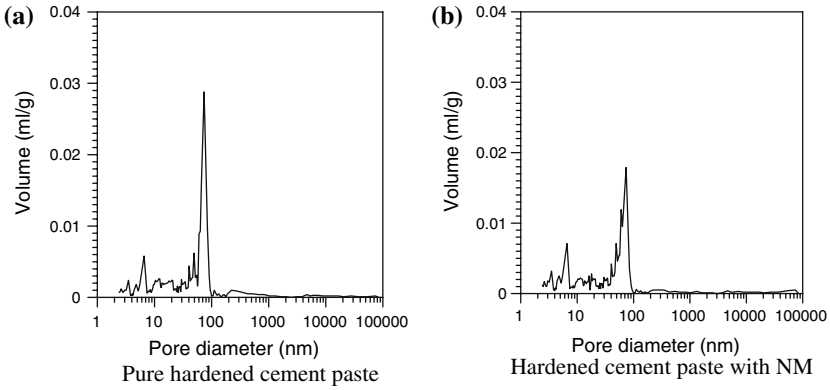

Fig. 12 Typical MIP pore distribution curves of hardened Portland cement composite (**a**) without NM (**b**) with 0.6% added NM

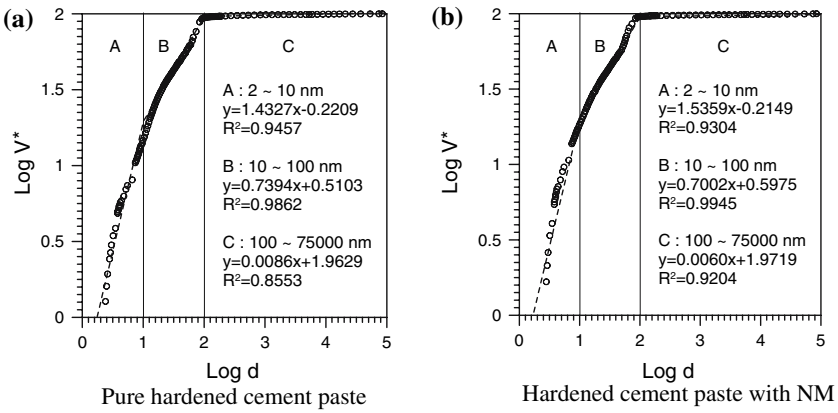

Fig. 13 Typical relation between volume ratio V^* and pore diameter d (nm) of Portland cement paste composite (**a**) without NM (**b**) with 0.6% added NM in log-log scale

k can be related to a fractal dimension D^* given as follows [32],

$$D^* = 3 - k \tag{10}$$

Practically, the range of fractal dimension D^* of the pore structure of hardened cement paste is between 0 and 3 and is influenced by the various factors such as the degree of hydration of cement paste, the water-to-cement ratio, the addition of pozzolanic material, etc. Normally, the larger the value of D* of pore structure of hardened cement paste is, the higher the strength of hardened cement paste will be [33].

Based on locations of slope changes of curve, the abscissas in Fig. 13a and b are roughly divided into three zones A, B and C, where zone A denotes the pore size smaller than 10 nm, zone B the pore sizes between 10 nm and 100 nm and zone C the pore size larger than 100 nm. An independent least-square linear model to fit the test data at each of three zones was conducted to obtain the slope k

Table 6 Values of slope k, fractal dimension D^* and total volume ratio V_P at three zones

	Pure hardened Portland cement paste			Hardened Portland cement composite with 0.6% NM		
Zone Range	A < 10 nm	B 10~100 nm	C > 100 nm	A < 10 nm	B 10~100 nm	C > 100 nm
k	1.433	0.739	0.009	1.536	0.700	0.006
D^*	1.567	2.261	2.991	1.464	2.300	2.994
V_P	14.84%	79.31%	5.85%	18.48%	77.15%	4.37%

in Eq. (9) and thus the value of D^* in Eq. (10) as presented in Table 6. After adding NM into Portland cement composite, the total volume ratio V_P at zone A increases by 3.64%, but decreases by 2.16% and 1.48% for zones B and C, respectively. On the contrary, the value of D^* decreases from 1.567 to 1.464 for zone A, but increases from.2.261 to 2.300 for zone B and from 2.991 to 2.994 for zone C, respectively. These results indicate that the microstructure of hardened cement composite with NM becomes more dense at the regions where the pore size is larger than 10 nm, but becomes looser at regions where the pore size is smaller than 10 nm.

Conclusions

Based on experimental results and microstructural analyses presented in this study, the following conclusions can be drawn:

1. After the age of 28 days, optimal amounts of added nano-montmorillonite into the cement paste are found to be 0.6% and 0.4% by weight of cement, in which the cement paste composites have the highest compressive strength and the lowest permeability coefficient. Meanwhile, the addition of nano-montmorillonite into the Portland cement paste has shown a better improvement on the permeability coefficient than the compressive strength. For example, at the age of 56 days, the cement composite with 0.1% of added nano-montmorillonite increases the permeability coefficient by 12.49%, but only increases by 2.21% for compressive strength.
2. The indices from various microstructural analyses, such T_g, α, Q^2/Q^1, FWHM and D^*, have indicated that the microstructures of Portland cement composite with nano-montmorillonite have become more dense and developed a more stable bonding structures. These improvements can enhance the durability of cement composite.
3. Although, the addition of nano-montmorillonite to the Portland cement paste has shown some improvement on the material properties, it seems that a longer elapsed time is still needed to develop its final prospective potential. Further research on subtle improvements in the manufacture of better Portland cement composite, such as the technique of dispersion, curing condition, mixing ingredients, etc., is definitely necessary.

Acknowledgements This work was performed under the auspices of the NSC, Taiwan, under Contract NSC-92–2211-E-011–052 which is highly appreciated.

References

1. Jortner J, Rao CNR (2002) Pure Appl Chem 74:1491
2. Pitkethly MJ (2004) Material Today 7:20
3. Dellisanti F, Valdre G (2005) Appl Clay Sci 28:233
4. Ahn T, Desai CS (1999) Inter J for Num Ana Meth In Geo 23:1893
5. Ryan CR, Day SR (2002) Geo Spec Pub 1161:713
6. Fukushima Y, Inagaki S (1987) J Inclu Phen 5:473
7. Kojima Y, Usuki A, Kawasumi M, Okada A, Fukushima Y, Kurauchi T, Kamigaito O (1993) J Mater Res 8:1185
8. Lebaron PC, Wang Z, Pinnavaia TJ (1999) Appl Clay Sci 15:11
9. Giannelis E (1996) Adv Mater 8:29
10. Alexandre M, Dubois P (2000) Mater Sci Eng 28:1
11. Taylor HFW (2000) Cement chemistry. Academic Press, London, p 305
12. Zhang X, Chang W, Zhang T, Ong CK (2000) J Am Cera Soc 83:2600
13. He C, Makovicky E, Osbaeck B (1996) Appl Clay Sci 10:351
14. Cabrera JG, Lynsdale CJ (1988) Mag Conc Res 40:177
15. Picandet V, Khelidj A, Bastian G (2001) Cem Conc Res 31:1525
16. Loosveldt H, Lafhaj Z, Skoczylas F (2002) Cem Conc Res 32:1357
17. Alshamsi AM, Imran HDA (2002) Cem Conc Res 32:923
18. Dhir RK, Hewlett PC, Chan NY (1989) Mag Conc Res 41:87
19. Joint Committee on Powder Diffraction Standards, JCPDS-International center for diffraction data (2000)
20. Sha W, O'Neill EA, Guo Z (1999) Cem Concr Res 29:1487
21. Sha W, Pereira GB (2001) Cem Concr Comp 23:455
22. Kurajica S, Bezjak A, Tkalcec E (1996) Therm Acta 288:123
23. Lippmaa E, Magi M, Samoson A, Engelhardt G, Grimmer AR (1980) J Am Ceram Soc 102:4889
24. Ida T, Hibino H, Toraya H (2001) J Appl Cryst 34:144
25. Justnes H, Meland I, Bjoergum JO, Krane J, Skjetne T (1989) SINTEF FCB Report, p 1
26. Johansson K, Larsson C, Antzutkin ON, Forsling W, Kota HR, Ronin V (1999) Cem Concr Res 29:1575
27. Cong X, Kirkpatrick RJ (1996) Adv Cem Bas Mat 3:133
28. Winslow DN (1984) Surf Colloid Sci 13:259
29. Good RJ (1984) Surf Colloid Sci 13:283
30. Jenkins RG, Rao MB (1984) Powder Technol 38:177
31. Winslow DN, Diamond S (1970) J Mater 5:564
32. Ji X, Chan SYN, Feng N (1997) Cem Concr Res 27:1691
33. Indelicato F (1990) Mater Struct 23:289